EUROPEAN TRANSACTIONS ON TELECOMMUNICATIONS
Eur. Trans. Telecomms. (2008)
Published online in Wiley InterScience
(www.interscience.wiley.com) DOI: 10.1002/ett.1337

Transmission Systems

ML frequency synchronisation for OFDM systems in the presence of overlapped narrow band transmission systems

Mohamed Marey* and Heidi Steendam†

DIGCOM Research Group, TELIN Dept., Ghent University, Sint-Pietersnieuwstraat 41, 9000 Gent, Belgium

SUMMARY

Spectrum-overlay scenarios for wideband orthogonal frequency division multiplexing (OFDM) systems bring along new technical challenges that must be considered during the system design. In such a scenario, the receiver has to perform actions, such as channel estimation and synchronisation, in the presence of possibly strong in-band interference. In this paper, we derive the data-aided maximum likelihood (ML) fractional frequency estimator in the presence of narrow band interference (NBI) signals. Based on the ML algorithm which has a high complexity, we propose a number of simplifications to develop a lower complexity algorithm. The susceptibility of the simplified estimator to NBI signals is investigated in an analytical way. The analytical results are verified by means of simulations. Although the simplified estimator turns out to be essentially independent of the bandwidth and the location of the interferers, the performance of the estimator is very sensitive to the signal-to-interference ratio and the number of interferers. In contrast with the simplified estimator, simulation results indicate that the exact ML estimator is independent of the NBI signals. Copyright © 2008 John Wiley & Sons, Ltd.

1. INTRODUCTION

The orthogonal frequency division multiplexing (OFDM) transmission technique has received wide spread interest due to its high data rate transmission capability. The ease of implementation and the robustness to multipath channels that OFDM provides, have led to its acceptance in many applications such as digital video/audio broadcasting, wireless local area networks (LANs) and high speed digital subscriber lines [1–4]. However, OFDM is not without drawbacks. One important drawback in OFDM is its sensitivity to a carrier frequency offset (CFO) arising from Doppler shifts and/or oscillator instabilities [5]. A CFO results in a shift of the received signal spectrum in the frequency domain. The CFO can be divided into an integer and a fractional part with respect to the OFDM sub-carrier spacing δf. A non-zero integer part of the CFO yields a bit error rate equal to 0.5 [6]. The fractional CFO leads to a reduction of the signal amplitude and to a loss of sub-carrier orthogonality. The latter introduces inter-carrier interference (ICI) which results in a degradation of the global system performance. To maintain the useful signal to ICI ratio of 20 dB or more, the fractional CFO must be limited to 4% or less of the sub-carrier spacing [7].

Sometimes, scarcity of available bandwidth necessitates spectrum sharing between the OFDM system and other narrow band (NB) systems. The broadband very high frequency (B-VHF) project [8, 9], which aims to develop a new integrated broadband VHF system for aeronautical voice and data link communication based on multi-carrier technology, is a good example of an overlay system. In this project, the OFDM system is intended to share parts of the VHF spectrum which are currently used by NB systems such as voice DSB-AM systems and VHF digital links. Further,

* Correspondence to: Mohamed Marey, DIGCOM Research Group, TELIN Dept., Ghent University, Sint-Pietersnieuwstraat 41, 9000 Gent, Belgium.
E-mail: mohamed@telin.ugent.be
† Senior Member, IEEE.

Received 22 September 2006
Revised 19 May 2008
Accepted 8 September 2008

an OFDM system is now applied in some unlicensed frequency bands, e.g. the Industrial-Scientific-Medical (ISM) band in 2.4 GHz and the Unlicensed National Information Infrastructure band (UNII) in 5.2 GHz [10]. However, since the frequency bands are unlicensed, there may exist many different wireless systems, such as wireless LANs, cordless phones and Blue-tooth piconets, sharing the same frequency band. If a part of the spectrum of the OFDM system is overlapped by a relatively narrow band transmission signal, the latter will introduce narrow band interference (NBI), which hampers the proper action of the OFDM system. In such scenarios, the OFDM receiver has to perform actions, such as channel estimation and synchronisation, in the presence of possibly strong in-band interference.

Generally, there are three basic models of NBI signals: (1) the tonal model; (2) the narrow band digital communication model; (3) the ergodic narrow band stochastic processes model. Tonal NBI signals consist of the sum of pure unmodulated complex sinusoidal signals. It is an accurate model for carrier feed-through, which arises from the I/Q modulators of the transmitter, tone jammers, narrow band FM cordless telephones, baby monitors and garage door openers. The more general narrow band digital communication model also includes digitally modulated carriers. On the other hand, less structure can be assumed by modelling the NBI signals as ergodic narrow band stochastic processes, such as narrow band auto-regressions. Such processes do not have a specific deterministic structure.

Coulson investigated the effect of NBI, based on the tonal model, on pilot symbol detection and frequency synchronisation for OFDM systems [11]. However, his tonal model is not sufficient to describe interference sources with a bandwidth that is larger than a small fraction of the sub-carrier spacing of the OFDM system as occurs in the spectrum overlay scenarios. According to our best knowledge, no previous research was done to investigate the impact of digitally modulated NBI signals, which originate from other communication systems residing in the OFDM spectrum, on the performance of the OFDM system. This motivated us to study the effect of these digitally modulated NBI signals on the different parts of the OFDM receiver. For example, in References [12, 13], we have investigated the effect of digitally modulated NBI signals on symbol timing and integer frequency synchronisation for an OFDM system. The results of References [12, 13] indicate that the performance of the timing and frequency synchronisers for OFDM systems is strongly affected by the NBI signals.

In this paper, the effect of NBI on the performance of the data-aided maximum likehood (ML) fractional CFO estimator for the OFDM system is investigated. The paper is organised as follows. The system model is addressed in Section 2. In Section 3, we derive the ML fractional CFO estimator for the OFDM system in the presence of NBI. Further, we propose two simplifications of the ML estimator that have lower complexity than the optimal ML estimator. Also, the susceptibility of the simplified ML estimator is investigated in an analytical way. The simulation and analytical results are discussed in Section 4. Finally, conclusions are given in Section 5.

2. SYSTEM DESCRIPTION

The model of the OFDM system including the NBI signals is depicted in Figure 1. In the OFDM transmitter, frames consisting of M_s OFDM blocks are transmitted. Each frame is generated as follows (see Figure 1): a block $\mathbf{z}_i = [z_{0,i}, \ldots, z_{N_z-1,i}]^{\mathrm{T}}$ of N_z information-bits is mapped to a sequence of N_u symbols, belonging to a 2^h- point constellation Ω (with $N_u = N_z/h$). We denote this sequence $\mathbf{d}_i = [d_{0,i}, \ldots, d_{N_u-1,i}]^{\mathrm{T}}$. The M_s blocks are buffered and converted, one at a time, to OFDM blocks

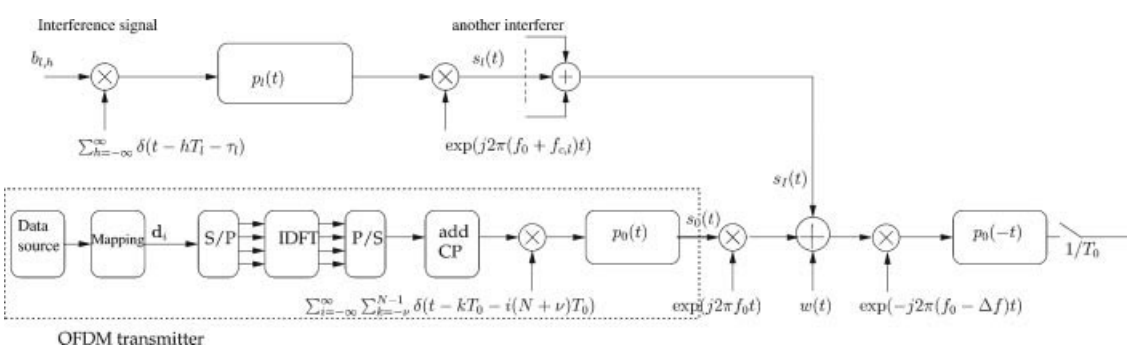

Figure 1. Block diagram of the OFDM system including interfering signals.

DOI: 10.1002/ett

by using an N-point inverse discrete Fourier transform (IDFT), where $N \geqslant N_u$. A ν-point cyclic prefix (CP) is pre-appended, resulting in $N+\nu$ time domain samples $[s_{-\nu,i}, \ldots, s_{-1,i}, s_{0,i}, \ldots, s_{N-1,i}]^{\mathrm{T}}$ where $s_{k,i} = s_{k+N,i}$ for $k = -\nu, \ldots, -1$ and $i = 0, \ldots, M_s - 1$. The kth time domain sample of the ith OFDM data block can be written as

$$s_{k,i} = \sqrt{\frac{1}{N+\nu}} \sum_{n \in I_u} d_{n,i}\, \mathrm{e}^{\frac{j2\pi kn}{N}} \quad -\nu \leqslant k \leqslant N-1 \quad (1)$$

where I_u is a set of N_u sub-carrier indices and $d_{n,i}$ is the nth data symbol of the ith OFDM block; the data symbols are independently and identically distributed random values with zero mean and variance $\mathrm{E}[|d_{n,i}|^2] = \sigma_d^2$. The energy per data symbol E_s is given as

$$E_s = \sigma_d^2 T_0 = \frac{2\sigma_s^2 (N+\nu) T_0}{N_u} \quad (2)$$

where σ_s^2 is the variance of the real/imaginary part of $s_{k,i}$ and T_0 is the sample duration.

Each data frame is preceded by one OFDM pilot block ($i = -1$), to be able to synchronise the receiver. The pilot block has two identical halves in the time domain, which will remain identical after passing through the channel, except that there will be a phase difference between them caused by the carrier frequency offset. The symmetry in the time domain of the pilot block is easily generated by transmitting a pseudonoise (PN) sequence on the even frequencies, while zeros are used on the odd frequencies. In order to maintain an approximately constant energy for each OFDM block (in the pilot block, only half of the sub-carriers are modulated whereas in the data blocks all sub-carriers are modulated), the energy per symbol of the pilot block is multiplied by an appropriate scaling.

Finally, the baseband OFDM time domain signal $s_0(t)$ consists of the concatenation of all time domain data and pilot blocks:

$$s_0(t) = \sum_{i=-1}^{M_s-1} \sum_{k=-\nu}^{N-1} s_{k,i}\, p_0(t - kT_0 - i(N+\nu)T_0) \quad (3)$$

where $p_0(t)$ is the transmit filter of the OFDM system. The baseband signal (3) is up-converted to the radio frequency f_0. At the receiver, the signal is first down-converted to $-(f_0 - \Delta f)$, where Δf represents the frequency difference between the transmitter and receiver oscillators, then fed to the matched filter and finally sampled at rate $1/T_0$.

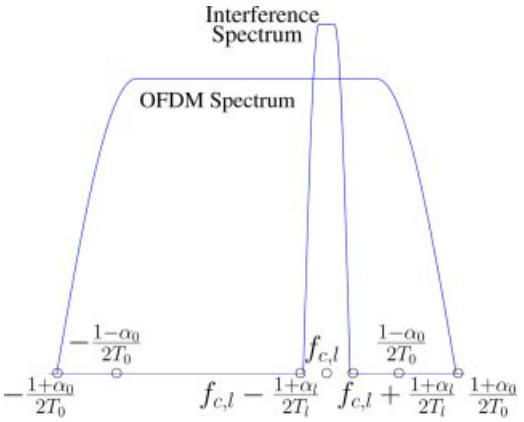

Figure 2. Baseband OFDM and one interfering signal spectrum.

The OFDM signal is disturbed by additive white Gaussian noise with uncorrelated real and imaginary parts, each having variance σ_n^2. The signal to noise ratio (SNR) at the output of the matched filter is defined as $\frac{\sigma_s^2}{\sigma_n^2}$.

Further, the OFDM signal is disturbed by the NBI signal residing within the same frequency band as shown in Figure 2. The interfering signal $s_I(t)$ can be described as

$$s_I(t) = \sum_{l=1}^{N_I} s_l(t)\, \mathrm{e}^{j2\pi(f_0 + f_{c,l})t} \quad (4)$$

where $s_l(t)$ is a baseband narrow band signal and $f_{c,l}$ is the carrier frequency deviation from f_0 for the lth interferer. The baseband interference signal $s_l(t)$ is modelled as a digitally modulated signal

$$\begin{aligned} s_l(t) &= \sum_{h=-\infty}^{\infty} b_{h,l}\, p_l(t - hT_l - \tau_l) \quad (5) \\ &\approx \sum_{h=0}^{q_l-1} b_{h,l}\, p_l(t - hT_l - \tau_l) \end{aligned}$$

where $p_l(t)$ is the transmit filter of the lth interferer, $b_{h,l}$ the hth interfering data symbol of the lth interferer, τ_l is its delay and $1/T_l$ its sample rate. We assume that only a limited number of q_l data symbols of the lth interferer have a relevant effect on the OFDM block; the integer number q_l is smaller than or equal to B_l/B_0, where B_l is the bandwidth of $p_l(t)$ and B_0 is the bandwidth of $p_0(t)$. Without loss of generality, we restrict our attention to the 0th OFDM block ($0 \leqslant t \leqslant T_{\mathrm{DFT}}$), i.e. only the symbols $b_{0,l}$, $b_{1,l}$, ..., $b_{q_l-1,l}$ are taken into account, resulting in the approximation in the second line of (5). The total NBI signal at the output of the

DOI: 10.1002/ett

OFDM matched filter is given by

$$r_I(t) \approx \sum_{l=1}^{N_I} \sum_{h=0}^{q_l-1} b_{h,l}\, \mathrm{e}^{j2\pi f_{c,l} h T_l} g_l(t - hT_l) \tag{6}$$

where $g_l(t)$ is the convolution of $p_0(-t)$ and $p_l(t - \tau_l)\exp(j2\pi(f_{c,l} + \Delta f)t)$. The normalised location of the interferer within the OFDM spectrum is defined as $f'_{c,l} = (\frac{f_{c,l}+\Delta f}{B_0})$. It is assumed that the interfering symbols are uncorrelated with each other, i.e. $\mathrm{E}[b_{h,l} b^*_{h',l'}] = \sigma_l^2 \delta_{ll'} \delta_{hh'}$ and $E_l = \sigma_l^2 T_l$. Further, the interfering data symbols $b_{h,l}$ are statistically independent of the OFDM data symbols $d_{n,i}$. The signal to interference ratio (SIR) at the input of the receiver is defined as [12, 13]

$$\mathrm{SIR} = \frac{2\sigma_s^2/T_0}{\sum_{l=1}^{N_I} \sigma_l^2/T_l} \tag{7}$$

3. ML FRACTIONAL CFO ESTIMATOR

As the frequency offset Δf is generally larger than the sub-carrier spacing, it is useful to split it into an integer part m and a fractional part ϵ with respect to the sub-carrier spacing $\delta f = \frac{1}{NT_0}$, i.e. $\Delta f = \frac{m}{NT_0} + \frac{\epsilon}{NT_o}$ where $\epsilon \in [-0.5, 0.5]$. We assume that the parameter m has already been estimated and corrected. The received time domain samples outside the CP are given by

$$\begin{aligned} y(k) &= \mathrm{e}^{j(2\pi\epsilon k/N)} x(k) + w(k) + r_I(k) \\ &\forall k = 0, \ldots, N-1 \end{aligned} \tag{8}$$

where $x(k)$ denote the samples of the transmitted signal $s_0(t)$ within the training block interval after convolution with the channel impulse response, $w(k) \sim N(0, 2\sigma_n^2)$[‡] and $r_I(k)$ is the interference contribution at sample time kT_0 as given in (6). We introduce two vectors of length $N/2$: $\mathbf{y}_1 = [y_1(0), \ldots, y_1(N/2-1)]^{\mathrm{T}}$ consists of the first half of the pilot block, i.e. $y_1(k) = y(k)$. Similarly, $\mathbf{y}_2 = [y_2(0), \ldots, y_2(N/2-1)]^{\mathrm{T}}$ consists of the second half of the pilot block, i.e. $y_2(k) = y(k + N/2)$. Taking into account that $x(k) = x(k + N/2)$, we find

$$\begin{aligned} y_2(k) = {} & y_1(k)\, \mathrm{e}^{j\pi\epsilon} + w\,(k + N/2) - w(k)\, \mathrm{e}^{j\pi\epsilon} \\ & + r_I\,(k + N/2) - r_I\,(k)\ \mathrm{e}^{j\pi\epsilon} \end{aligned} \tag{9}$$

where $k = 0, \ldots, N/2-1$. Assuming that the noise and the interference components are Gaussian random variables, the distribution of $\mathbf{y}_2$ given $\mathbf{y}_1$ and ϵ yields

$$\begin{aligned} P\,(\mathbf{y}_2 \,|\, \mathbf{y}_1, \tilde{\epsilon}) = {} & \frac{1}{\pi^{N/2}\,|C_x|} \cdot \exp\Big\{ - \left(\mathbf{y}_2 - \mathbf{y}_1\, \mathrm{e}^{j\pi\tilde{\epsilon}}\right)^H \\ & \times \mathbf{C}_{\mathbf{x}}^{-1} \left(\mathbf{y}_2 - \mathbf{y}_1\, \mathrm{e}^{j\pi\tilde{\epsilon}}\right) \Big\} \end{aligned} \tag{10}$$

where $\tilde{\epsilon}$ is the trial value of ϵ and $\mathbf{C}_{\mathbf{x}}$ is the covariance matrix given by

$$\begin{aligned} [\mathbf{C}_{\mathbf{x}}]_{k,k'} &= \mathrm{E}\Big[\left(y_2(k) - y_1(k)\, \mathrm{e}^{j\pi\epsilon}\right) \cdot \left(y_2(k') - y_1(k')\, \mathrm{e}^{j\pi\epsilon}\right)^* \Big] \\ &= 4\sigma_n^2 \delta_{kk'} + A(k,k') + A(k + N/2, k' + N/2) \\ &\quad - A(k, k' + N/2)\, \mathrm{e}^{j\pi\epsilon} - A^*(k + N/2, k')\, \mathrm{e}^{-j\pi\epsilon} \end{aligned} \tag{11}$$

where $A(k, k')$ is defined as

$$A(k,k') = \sum_{l=1}^{N_I} \sigma_l^2 \sum_{h=-\infty}^{\infty} g_l(kT_o - hT_l) g_l^*(k'T_o - hT_l) \tag{12}$$

Dropping irrelevant terms from (10), we get the likelihood function $\Lambda(\tilde{\epsilon})$:

$$\Lambda(\tilde{\epsilon}) = \Re\left\{ \mathbf{y_1}^H \mathbf{C}_{\mathbf{x}}^{-1} \mathbf{y_2}\, \mathrm{e}^{-j\pi\tilde{\epsilon}} \right\} \tag{13}$$

The estimated value $\hat{\epsilon}$ of ϵ maximises $\Lambda(\tilde{\epsilon})$. Taking the derivative of (13) with respect to $\tilde{\epsilon}$ and setting the result to zero yields

$$\hat{\epsilon} = \frac{1}{\pi} \arctan \frac{\Im\left\{ \mathbf{y_1}^H \mathbf{C}_{\mathbf{x}}^{-1} \mathbf{y_2} \right\}}{\Re\left\{ \mathbf{y_1}^H \mathbf{C}_{\mathbf{x}}^{-1} \mathbf{y_2} \right\}} \tag{14}$$

where $\Re\{x\}$ and $\Im\{x\}$ are the real and imaginary parts of the complex number x. This estimator[§] (14) requires the knowledge of the second order statistics of the NBI to compute the matrix $\mathbf{C}_{\mathbf{x}}$. Further, it requires the inversion of $\mathbf{C}_{\mathbf{x}}$. Therefore, the complexity of this estimator might be too high. To simplify the estimator (14), we take a closer look at the matrix $\mathbf{C}_{\mathbf{x}}$. The function $A(k, k')$ represents the sum of the

[‡] $w(k) \sim N(0, 2\sigma_n^2)$ means that $w(k)$ is Gaussian distributed with average 0 and variance $2\sigma_n^2$.

[§] Note that in this pilot-based ML estimator only the repetition of the two identical halves of the pilot OFDM block is used, and not the knowledge of the pilots itself. Therefore, the proposed algorithm is not the true data-aided ML algorithm.

DOI: 10.1002/ett

Figure 3. $A(k, k')$ for N_I=1, $f'_{c,1}$=0, B_l/B_0=0.0244 and σ_1^2=1.

product of the interferer pulse after matched filtering with its delayed version over an integer number of sample intervals T_0. In Figure 3, the matrix $\mathbf{C_x}$ is shown as an image for $N = 1024$, one interferer with $f'_{c,1} = 0$, $\sigma_1^2 = 1$, a normalised interference bandwidth $B_l/B_0 = 0.024$, and SNR $= \infty$. A lighter colour corresponds to larger components of $\mathbf{C_x}$ and a dark colour corresponds to small values (nearly zero) of $\mathbf{C_x}$ components. It is clear from the figure that the larger elements of $\mathbf{C_x}$ occur at the main sub-diagonals. The further away the elements are from the main diagonal, the smaller the elements will be. Therefore, we suggest two types of approximations to simplify the inversion of the matrix $\mathbf{C_x}$. In the first approximation, we assume that most of the $\mathbf{C_x}$ elements are zero except for $2M$ sub-diagonals around the main diagonal (i.e. M sub-diagonals at each side of the main diagonal, such that $2M + 1$ sub-diagonals have non-zero components). In the second approximation, we neglect the all interference components in the covariance matrix. In this case, $\mathbf{C_x}$ becomes a diagonal matrix with diagonal value $4\sigma_n^2$, and the estimator (14) can be simplified as

$$\hat{\epsilon} = \frac{1}{\pi} \arctan \frac{\Im\left\{\sum_{k=0}^{N/2-1} y_1^*(k) y_2(k)\right\}}{\Re\left\{\sum_{k=0}^{N/2-1} y_1^*(k) y_2(k)\right\}} \tag{15}$$

Implementation Aspects

- From Figure 3, we notice that $[\mathbf{C_x}]_{k,k'}$ sharply drops when $k \neq k'$ and $|k - k'| > N/4$. Therefore, for all significant elements of $[\mathbf{C_x}]_{k,k'}$, i.e. for $|k - k'| < N/4$, $|A(k, k') + A(k + N/2, k' + N/2)|$ is larger than $|A(k, k' + N/2)\,\mathrm{e}^{j\pi\epsilon} - A^*(k + N/2, k')\,\mathrm{e}^{-j\pi\epsilon}|$ so that we can say that $[\mathbf{C_x}]_{k,k'}$ is essentially independent of the fractional frequency offset ϵ, see (11). Hence, if the statistics of the NBI signals are known, the matrix $\mathbf{C_x}^{-1}$ can be precomputed and stored at the receiver. Accordingly, we do not need to re-estimate $\mathbf{C_x}^{-1}$ every frame.
- If the statistics of the NBI signals are not known, we can use estimator (15), where the NBI effect is neglected.

Now, we evaluate analytically the effect of the NBI on the simplified estimator (15). Due to the presence of the inverse of the tangent function, it is difficult to compute the mean and the variance of $\hat{\epsilon}$ directly. To simplify, as in Reference [7], we assume that $|\hat{\epsilon} - \epsilon|$ is small enough to approximate the tangent by its argument

$$\tan\left[\pi\left(\hat{\epsilon} - \epsilon\right)\right] \approx \pi\left(\hat{\epsilon} - \epsilon\right) = \frac{\Im\left\{\mathbf{y}_1^H \mathbf{y}_2\,\mathrm{e}^{-j\pi\epsilon}\right\}}{\Re\left\{\mathbf{y}_1^H \mathbf{y}_2\,\mathrm{e}^{-j\pi\epsilon}\right\}} \tag{16}$$

At high SNR and SIR values, $\Re\{y_2(k)y_1^*(k)\,\mathrm{e}^{-j\pi\epsilon}\}$ can be approximated by $|x(k)|^2$ as the noise and interference components are much smaller than the signal component. Also, it is easy to prove that $\mathrm{E}[\Im\{\mathbf{y}_1^H \mathbf{y}_2\,\mathrm{e}^{-j\pi\epsilon}\}] = 0$. Then, $\mathrm{E}[\hat{\epsilon}] = \epsilon$, i.e. the estimator is unbiased. The variance of the estimate is straightforward determined from (16) as

$$\mathrm{E}\left[(\hat{\epsilon} - \epsilon)^2\right] \approx \frac{2}{\pi^2 N^2 \sigma_s^4}\left(\frac{N}{2}\left(2\sigma_s^2\sigma_n^2 + \sigma_n^4\right) + \left(\sigma_s^2 + \sigma_n^2\right)\Upsilon + \Gamma\right) \tag{17}$$

where Υ and Γ are given by

$$\Upsilon = \sum_{k=0}^{N/2-1} \{A(k, k) + A(k + N/2, k + N/2)\} \tag{18}$$

$$\Gamma = \sum_{k,k'=0}^{N/2-1} A(k, k) A(k' + N/2, k' + N/2) \tag{19}$$

In the next section, we evaluate the performance of the exact and the simplified ML estimators given by (14) and (15), respectively, by means of simulations.

4. NUMERICAL RESULTS

The numerical results in this paper are obtained with the following OFDM and interference parameters:

DOI: 10.1002/ett

- The transmit filters are square-root raised-cosine filters with roll off factors $\alpha_0 = 0.25$ and $\alpha_l = 0.5$ for OFDM and interfering signals, respectively.
- The total number of sub-carriers is $N = 1024$.
- The number of active sub-carriers is $N_u = 1000$.
- The guard interval is set to about 10% of the useful part, $\nu = 102$.
- The bandwidth of the OFDM spectrum equals $B_0 = \frac{1}{T_0} = 1024\,\text{kHz}$.
- We use QPSK modulation for the data symbols of the OFDM and the interferer signals.
- The time delay of the interferers equals $\tau_l = 0$.

Figure 4 compares the analytical results (17) with the simulations of the mean square error (MSE) of the simplified ML estimator (15), as function of the SIR. As can be observed, for a large range of the SIR, the theoretical results and the simulation results agree well. The MSE of the simplified ML estimator is a decreasing function of the SIR, and reaches an asymptote at large SIR, corresponding to the case where no interference is present. This asymptote is determined by neglecting in (17) the interference components. Taking into account that $\text{SNR} = \sigma_s^2/\sigma_n^2$, the asymptote equals $\frac{2\sigma_s^2\sigma_n^2+\sigma_n^4}{\pi^2 N\sigma_s^4} \approx \frac{2}{\pi^2 N\,\text{SNR}}$. Hence, the MSE at high SIR reduces for increasing SNR. This can easily be explained as at high SIR and SNR, the effect of the noise and interference is small. At low SIR, the MSE of the simplified estimator becomes independent of the SNR. The theoretical results are smaller than the simulations when the SIR is small. Hence, the theoretical results can be considered as a lower bound on the performance for small SIR.

Furthermore, in Figure 4 the simulated MSE of the exact ML estimator (14) is shown as function of the SIR

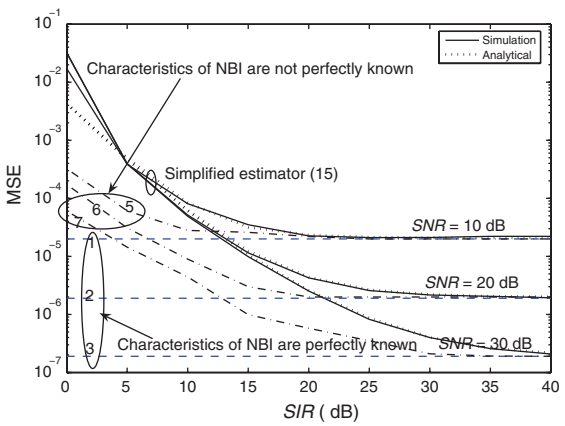

Figure 4. MSE of the estimator versus signal to interference ratio (SIR), $B_l/B_0 = 0.0244$, $f'_{c,1} = 0$ and $N_I = 1$.

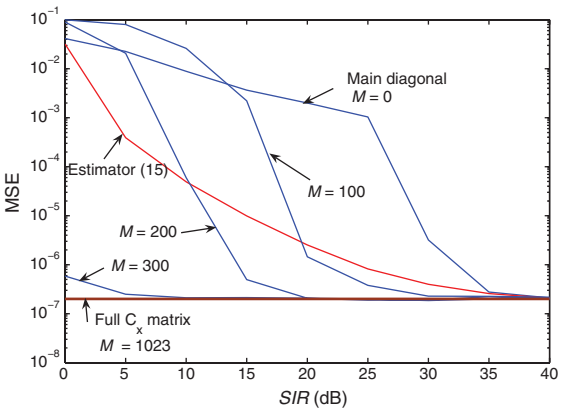

Figure 5. MSE as function of the SIR for different number of sub-diagonals, M ($N_I = 1$, $f'_{c,1} = 0$, $B_l/B_0 = 0.0244$ and SNR = 30 dB).

at different values of the SNR (curves (1, 2 , 3)) where we assume that the characteristics of the NBI signals, i.e SIR, B_l, $f'_{c,l}\ldots$, etc., are perfectly known. We note that the MSE of the exact ML estimator is independent of the SIR. Also, we consider another case where there is an uncertainty in the estimation of the NBI parameters. Let us assume that the covariance matrix $\mathbf{C_x}$ is calculated at $f'_{c,l} = 0$, while the actual value of $f'_{c,l}$ is $0.01B_1$. In this case, we observe that the simulated MSE of the exact ML estimator changes with the SIR as shown in curves (5, 6, 7). Hence, the exact estimator is very sensitive to uncertainties in the estimation of the NBI parameters.

Figure 5 shows the simulated MSE of the approximated ML estimator, where the matrix $\mathbf{C_x}$ is approximated by keeping beside the main diagonal, only $2M$ non-zero sub-diagonals around the main diagonal; all other elements of $\mathbf{C_x}$ are set to zero. As can be observed in the figure, the MSE decreases with increasing M: as expected, the closer the approximated matrix $\mathbf{C_x}$ is to the actual one, the better the performance we obtain, except for $M = 0$ at low SIR. This can be explained with the aid of Figure 3. As can be observed in Figure 3, the dominant elements of the $N \times N$ matrix $\mathbf{C_x}$ are located around the main diagonal, and at sub-diagonals at a distance of approximately $N/4$ from the main diagonal. By setting $M = 0$, only the main diagonal is kept, and many dominant elements of $\mathbf{C_x}$ are neglected, resulting in a very high MSE for almost all values of the SIR. When $M \geqslant N/4$ (in our figure $M \geqslant 256$), most dominant contributions of $\mathbf{C_x}$ are used, resulting in an acceptable performance for a wide range of the SIR. At high SIR, the approximated ML estimator has better performance

DOI: 10.1002/ett

than the simplified ML estimator[‖] (15). Indeed, at high SIR, the sub-diagonal elements of $\mathbf{C_x}$ will be very small as compared to the main diagonal elements, and can therefore be neglected. Furthermore, in the simplified ML estimator, the contribution of the NBI to the main diagonal is neglected. However, this contribution can only be neglected when the NBI is small as compared to the noise, i.e. when SIR $\geqslant$ SNR. Therefore, at high SIR, the approximated ML estimator outperforms the simplified ML estimator. The MSE of the approximated ML estimator increases when the SIR decreases. This can be explained as at low SIR, the absolute value of all the elements of $\mathbf{C_x}$ increases. Hence, the errors made in the approximation of $\mathbf{C_x}$ increase, causing an increasing MSE, such that more non-zero sub-diagonals are necessary to have an acceptable performance at low SIR: if the number of non-zero sub-diagonals is too small, the approximation errors will have an adverse effect and cause a dramatical MSE increase, such that the approximated ML estimator has worse performance than the simplified ML estimator. This also explains why the range of SIR over which the approximated ML estimator outperforms the simplified ML estimator increases for increasing M. Based on this figure, one can determine for a given SIR value how many non-zero sub-diagonals are necessary to obtain an acceptable performance.

Figure 6 displays the analytical and simulation results for the MSE of the simplified ML estimator as function of the normalised interference bandwidth B_l/B_0 for different values of the SIR. The results indicate that the dependency of the MSE on the normalised interference bandwidth increases when the SIR decreases, although the dependency is small. This is explained as at high SIR, the effect of interference diminishes and the MSE depends on the noise only. At low SIR, the MSE slightly increases for small normalised interference bandwidth. In this case, the pulse $g_l(t)$ has a longer duration, and hence the sum in (12) contains more terms, and its contribution to $\mathbf{C_x}$ will be larger. As this contribution is neglected in the simplified estimator, the error made is larger, resulting in a larger MSE. Furthermore, the MSE of the exact ML estimator is shown as function of B_l/B_0 at different SIR and turns out to be independent of the normalised interference bandwidth.

Figure 7 illustrates the analytical and simulation results of the MSE of the simplified ML estimator as function of

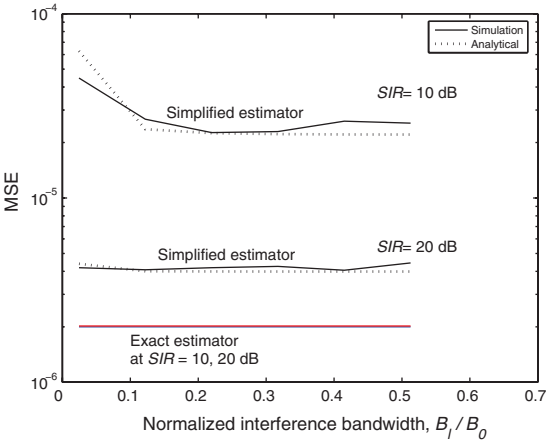

Figure 6. MSE versus normalised interference bandwidth, B_l/B_0 ($f'_{c,1} = 0$ and $N_I = 1$ and SNR $= 20$ dB).

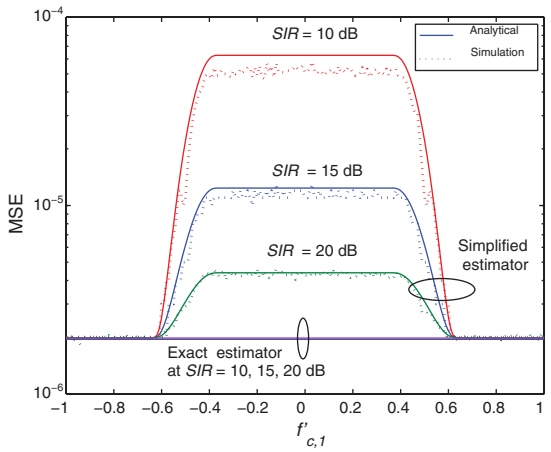

Figure 7. MSE versus normalised interference carrier frequency, $f'_{c,1}$ (SNR $= 20$ dB, $B_l/B_0 = 0.0244$ and $N_I = 1$).

the normalised interference carrier frequency deviation $f'_{c,l}$. The shape of the MSE can be explained with the aid of Figure 2. As long as the interfering signal is located in the flat region of the OFDM spectrum, i.e $\left|f_{c,l} + \frac{(1+\alpha_l)}{(1+\alpha_0)}\frac{T_0}{T_l}\right| < \frac{1-\alpha_0}{1+\alpha_0}$, the MSE of the simplified ML estimator is constant and does not depend on the location of the interferer. When the interfering signal is located outside the OFDM bandwidth i.e. $\left(f_{c,l} + \frac{(1+\alpha_l)}{(1+\alpha_0)}\frac{T_0}{T_l} > 1 \text{ or } f_{c,l} - \frac{(1+\alpha_l)}{(1+\alpha_0)}\frac{T_0}{T_l} < -1\right)$, the interfering signal does not affect the OFDM signal anymore: in this region the MSE is constant and its value depends on the SNR value only. Further we show the MSE of the exact ML estimator: it is independent of $f'_{c,l}$.

[‖] The approximated ML estimator with $M = 0$ is not equal to the simplified ML estimator, as in the latter, all NBI contributions in $\mathbf{C_x}$ are neglected, whereas in the former, the main diagonal elements still contain a contribution from the NBI.

DOI: 10.1002/ett

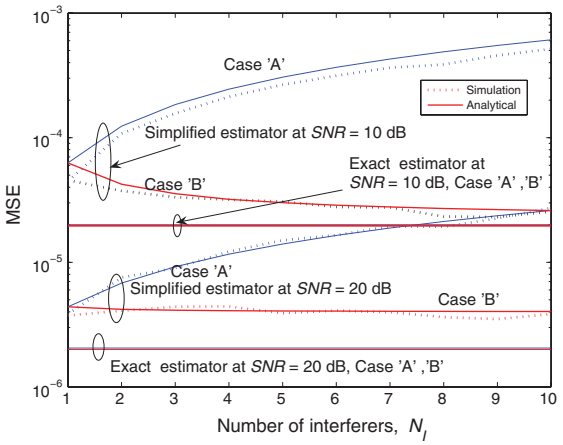

Figure 8. MSE versus number N_I of interference signals ($B_I/B_0 = 0.0244$, SIR $= 20$ and SNR $= 20$ dB).

Figure 8 shows the MSE of the simplified ML estimator as function of the number of interfering signals, N_I, in two cases, where we assume that the N_I interferers are uniformly distributed over the OFDM spectrum. In case 'A', we consider that the SIR is fixed per interferer, so the total SIR decreases inversely proportional to N_I. In case 'B', we consider a fixed total SIR, i.e. the SIR per interferer decreases linearly as N_I increases. As the MSE mainly depends on the total SIR (see Figure 4), it follows that the MSE will be an increasing function of the number N_I of interferers in case 'A', whereas it is independent of N_I in case 'B'. The MSE of the exact ML estimator is independent of the number N_I of interferers for both cases 'A' and 'B'. Taking into account the results of Figures 4–8, it turns out that the exact ML estimator is independent of the NBI.

5. CONCLUSIONS

This paper evaluates the performance of the ML fractional frequency estimator for an OFDM system in the presence of NBI signals. We derived the ML estimator based on a training block with two identical halves in the time domain. The complexity of the exact ML estimator is high, as it includes the inversion of a large matrix $\mathbf{C_x}$ that changes from OFDM block to OFDM block. Therefore, we proposed two lower complexity approximations: the simplified ML estimator, where all NBI contributions are neglected in the estimation algorithm, and the approximated ML algorithm, where the matrix $\mathbf{C_x}$ is approximated by a matrix with only $2M + 1$ non-zero sub-diagonals. The performance of the estimators is evaluated analytically and/or through simulations. The agreement between the theoretical results and the simulations proves the validity of our analysis. The exact ML estimators turns out to be independent of the NBI, whereas the two approximated lower complexity estimators strongly depend on the SIR: at low SIR, the simplified ML estimator fails, whereas the approximated ML estimator needs a large number non-zero sub-diagonals to have an acceptable performance.

ACKNOWLEDGEMENT

Mohamed Marey gratefully acknowledges the financial support of the Egyptian government.

REFERENCES

1. Bingham J. Multi-carrier modulation for data transmission: an idea whose time has come. *IEEE Communications Magazine* 1990; **28**(5): 5–14.
2. Sari H, Karam G, Jeanclaude I. Transmission techniques for digital terrestrial TV broadcasting. *IEEE Communications Magazine* 1995; **33**(2):100–109.
3. van Nee R, Awater G, Morikara M, Takanashi H, Webster M, Halford KW. New high-rate wireless LAN standards. *IEEE Communications Magazine* 1999; **37**(12):82–88.
4. Chow J, Tu J, Cioffi J. A discrete multi-tone transceiver system for HDSL applications. *IEEE Journal on Selected Areas in Communications* 1991; **9**(6):895–908.
5. Pollet T, Van Bladel M, Moeneclaey M. BER sensitivity of OFDM systems to carrier frequency offset and wiener phase noise. *IEEE Transactions on Communications* 1995; **43**(2):191–193.
6. Keller T, Hanzo L. Adaptive multi-carrier modulation: a convenient framework for time-frequency processing in wireless communications. *Proceedings of the IEEE* 2000; **88**(5):611–640.
7. Moose PH. A technique for orthogonal frequency division multiplexing frequency offset correction. *IEEE Transactions on Communications* 1994; **42**(10):2908–2914.
8. Schnell M, Haas E, Sajatovic M, Rihacek C, Haindl B. B-VHF—An overlay system concept for future ATC communications in the VHF band. In *Proceedings of the 23rd International Digital Avionics Systems Conference*, Salt Lake City, USA, October 2004.
9. http://www.b-vhf.org
10. Zhang D, Fan P, Cao Z. Interference cancellation for OFDM systems in presence of overlapped narrow band transmission system. *IEEE Transactions on Consumer Electronics* 2004; **50**(1):108–114.
11. Coulson AJ. Narrow band interference in pilot symbol assisted OFDM systems. *IEEE Journal on Selected Areas in Communications* 2004; **3**(6):2277–2287.
12. Marey M, Steendam H. Analysis of the narrow band interference effect on OFDM timing synchronization. *IEEE Transactions on Signal Processing* 2007; **55**(9):4558–4566.
13. Marey M, Steendam H. Analysis of the narrow band interference effect on frequency ambiguity resolution for OFDM systems. *European Transactions on Telecommunications*, 2008; DOI: 10.1002/ett.1273

AUTHORS' BIOGRAPHIES

Mohamed Marey received the B.Sc. and M.Sc. degrees in Electrical Engineering from Menoufyia University, Egypt, in 1995 and 1999 respectively. He worked as an instructor and assistant lecturer at the Department of Electronic and Communication Engineering, Menoufyia university in 1996–1999 and 1999–2004 respectively. Between 2004 and 2008, he served as a researcher at the Department of Telecommunications and Information Processing, Ghent University, Belgium, where he received the Ph.D degree in Electrical Engineering in June 2008. Since September 2008, he has worked as full time lecturer in the area of Digital Communications at the Department of Electronic and Communication Engineering, Menoufyia university.

Dr. Marey received the young scientist award from International Union of Radio Science (URSI) in 1999. He is the author of around 20 scientific papers published in international journals and conference proceedings. His main research interests include Synchronization, Channel Estimation and Equalization, Error Correcting Codes, Iterative Processing, Spread Spectrum, Multi-Input Multi-Output (MIMO), and Multi-Carrier communication systems.

Heidi Steendam received the M.Sc. degree in Electrical Engineering and the Ph.D. degree in Applied Sciences from Ghent University, Gent, Belgium in 1995 and 2000, respectively. Since September 1995, she has been with the Digital Communications (DIGCOM) Research Group, Department of Telecommunications and Information Processing (TELIN), Faculty of Engineering, Ghent University, Belgium, first in the framework of various research projects, and since October 2002 as a full time Professor in the area of Digital Communications. Her main research interests are in statistical communication theory, carrier and symbol synchronisation, bandwidth-efficient modulation and coding, spread-spectrum (multi-carrier spread-spectrum), satellite and mobile communication. She is the author of more than 80 scientific papers in international journals and conference proceedings. Since 2002, she is an executive Committee Member of the IEEE Communications and Vehicular Technology Society Joint Chapter, Benelux Section. She has been active in various international conferences as Technical Program Committee member and Session chair. In 2004, she was the conference chair of the IEEE Symposium on Communications and Vehicular Technology in the Benelux.

She is teaching courses on Data Communications, Information Theory and Advanced Modulation and Coding Techniques.

DOI: 10.1002/ett